Research Journal of Applied Sciences, Engineering and Technology 6(8): 1428-1445, 2013
DOI:10.19026/rjaset.6.3967
ISSN: 2040-7459; e-ISSN: 2040-7467
© 2013 Maxwell Scientific Publication Corp.
Submitted: October 22, 2012 Accepted: December 20, 2012 Published: July 10, 2013

Research Article

Nonlinear Dynamic Analysis of Multi-component Mooring Lines Incorporating Line-seabed Interaction

[1]V.J. Kurian, [2]M.A. Yassir, [3]C.Y. Ng and [4]I.S. Harahap
[1, 3, 4]Department of Civil Engineering, Universiti Teknologi PETRONAS Tronoh, Perak, Malaysia
[2]School of Civil Engineering, Sudan University of Science and Technology, Sudan

Abstract: In this study, a deterministic approach for the dynamic analysis of a multi-component mooring line was formulated. The floater motion responses were considered as the mooring line upper boundary conditions while the anchored point was considered as pinned. Lumped parameter approach was adopted for the mooring line modelling. The forces considered were the submerged weights of mooring/attachment, physical/added inertia, line tension, fluid/line relative drag forces and line/seabed reactive forces. The latter interactions were modelled assuming that the mooring line rested on an elastic dissipative foundation. An iterative procedure for the dynamic analysis was developed and results for various mooring lines partially lying on different soils were obtained and validated by conducting a comparative study against published results. Good agreement between numerical and published experimental results was achieved. The contribution of the soil characteristics of the seabed to the dynamic behaviour of mooring line was investigated for different types of soil and reported.

Keywords: Fluid drag force, lumped mass method, multi-component mooring line, moored floating structure, semi-submersible platform

INTRODUCTION

Traditionally, the inclusion of mooring line effects in the analysis of the motions of moored floating structures was carried out using the quasi-static methods (Thomas and Hearn, 1994). In this approach, the mooring line was assumed to respond statically to the environmental actions and floating platform motion excitation. This quasi-static behaviour of mooring systems was possible because the response of the mooring vessel was normally outside the frequency range of the mooring system. However, this kind of analysis ignored the effect of line dynamics, which in some situations may be a significant element in the dynamic analysis of a moored offshore vessel (Anasri, 2001). From both theoretical and experimental research, it was established that the dynamic behaviour of a mooring line induced by high frequency oscillations of the upper end contributed significantly to the line tensions and the motions (Boom, 1985).

In the mooring system design, a quasi-static analysis method was often used for evaluating the performance of a mobile mooring system and the effects of line dynamics were accommodated through the use of a relatively conservative safety factor. With the advent of moorings in very deep water, a more rigorous dynamic analysis was required for the final design of a permanent mooring system and the factor of safety was relaxed to remove some uncertainty in line tension prediction. Dynamic analysis accounted for the time varying effects due to mass, damping and fluid acceleration. In this approach, the time varying fairlead motions were calculated from the vessel's surge, sway, heave, pitch, roll and yaw motions. Dynamic models were used to predict the mooring line responses to the fairlead motions, as recognized by the American Petroleum Institute (API, 2005).

Two methods, frequency domain and time domain analyses were used for predicting dynamic mooring loads. In the time domain method, all nonlinear effects including line stretch, line geometry, fluid loading and sea bottom effects were modelled. On the other hand, the frequency domain method is always linear and the linear principle of superposition was used. Methods to approximate non-linear effects in the frequency domain and their limitations should be investigated to ensure acceptable solutions for the intended operation.

Most researchers adopt one of two methods, either Lumped Mass Method (LMM) or Finite Element Method (FEM). The LMM is the most widely adopted method (Hearn and Thomas, 1991). The application of LMM to the dynamic mooring problem was first applied by Walton and Polachech (1960). They provided some details of the formulation and solution techniques neglecting the mooring material elasticity, but information was given about the fluid reactive

Corresponding Author: V.J. Kurian, Department of Civil Engineering, Universiti Teknologi PETRONAS Tronoh, Perak, Malaysia
This work is licensed under a Creative Commons Attribution 4.0 International License (URL: http://creativecommons.org/licenses/by/4.0/).

forces and method validation. The explicit difference scheme was adopted to solve the problem with conditionally stable outputs. Other studies using this method (Thomas and Hearn, 1994; Anasri, 2001; Boom, 1985; Hearn and Thomas, 1991; Cho and Yi, 2002; Nakajima *et al*., 1982; Nakajima, 1986) gave a summary of the formulation and solution providing case studies and discussions. Nakajima *et al*. (1982) extended the model of Walton and Polachech (1960). They included material elasticity and seafloor lifting and grounding model neglecting the grounded part of the mooring line by forcing the first two suspended node masses that touched the seafloor to vanish.

This method involved lumping of all effects of mass, external forces and internal reactions at a finite number of points along the line. The behaviour of a continuous mooring line was modelled as a set of concentrated masses connected by mass-less springs. By applying the dynamic equilibrium conditions and equation of stress/strain continuity to each mass, a set of discrete equations of motion was derived. In this method, material damping, bending and torsional stiffness were usually neglected (Boom, 1985; Kreuzer and Wilke, 2003). This approach of modelling the mooring line basically resulted in the Partial Differential Equations (PDEs), which were replaced by a set of Ordinary Differential Equations (ODEs). The latter equations were solved in the time domain using an appropriate time integration scheme.

The FEM utilizes interpolation functions to describe the behaviour of a given internal variable to an element in terms of the displacements of the nodes in generalized co-ordinate system. The equations of motion for a single element are obtained by applying the interpolation functions to kinematic and constitutive relations and the equations of the dynamic equilibrium. The solution procedure is similar to the LMM. Various models based on the FEM have been presented either using linear or higher shape functions (Kreuzer and Wilke, 2003). The FEM has the advantage that it can be extended to analyse lines having significant bending and torsional stiffness amounts. But computer codes based on this method have lesser computation efficiency when compared with the LMM algorithms.

Problem definition: A Multi-Component Mooring Line (MCML) connected to a floating structure subjected to the environment consisting of wind, waves and current was subjected to line-end loads, weight, buoyancy, sea-floor reactive forces, line/attachments inertia and fluid reactive forces. The following assumptions were used in the mathematical problem formulation:

- The evaluation of the responses of the floating structure and the mooring to the environment excitation could be made separately since motions of the floating structure were not affected significantly by the mooring line tensions.
- The mooring line remained in the vertical plane through both ends and the anchor boundary condition was not allowed to respond to the applied forces. Hence the motions of the mooring fairleader represented the predefined upper node boundary condition for the analysis of the mooring line.
- The continuous distribution of mooring line mass was replaced by a discrete distribution of lumped masses at a finite number of points "nodes" where all internal and external forces were considered to act. These nodes were connected by a series of straight mass-less spring segments "elements".
- The forces considered were the element tensions (assumed to be constant per element); the global fluid loading, the seabed reactive forces, the inertia forces and effective weights, all lumped carefully at nodes.
- The mooring line rested on a bed of elastic foundation and the Touchdown Point (TDP) was a variable during the oscillating excitation.
- The line was fully flexible in the bending directions and only the secant stiffness of the line was considered in the analysis.
- The modified version of Morison's equation, which accounted for the relative fluid/line velocities, was sufficient for the evaluation of the hydro-dynamic forces. These forces were initially evaluated in the element local co-ordinates with special attention given for force transfer coefficients. Linear loading variation per element was assumed.
- The hydrodynamic force transfer coefficients were independent of the wave/ upper end motion excitation frequencies. Hence constant values of the hydrodynamic force transfer coefficients were adopted.

MATHEMATICAL FORMULATION

- **The Governing Equations of Motion (GEOM):** The mathematical model adopted in this study was a modification of the LMM given by Boom (1985). The mooring line was represented by a set of masses interconnected by springs as shown in Fig. 1. In order to derive the Governing Equations of Motion (GEOM) for the jth lumped mass, Newton's law of motion was applied in global system co-ordinates.

The nodal accelerations in the global coordinate system were resolved to the node local co-ordinate in terms of the node average angle $\bar{\theta}_j$, which was given by Eq. (1):

$$\bar{\theta}_j = \frac{1}{2}\left(\theta_{j-\frac{1}{2}} + \theta_{j+\frac{1}{2}}\right) \quad (1)$$

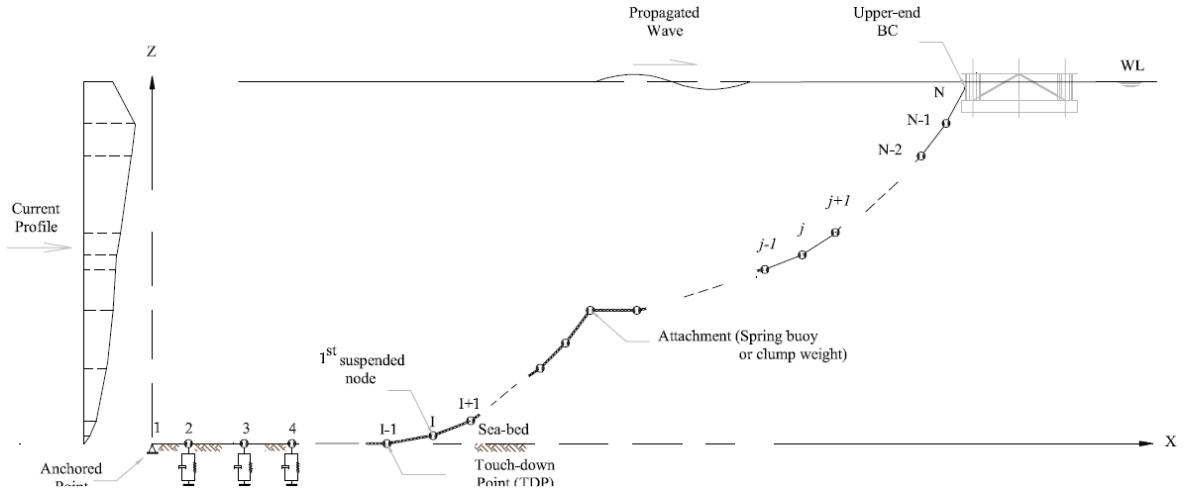

Fig. 1: Multi-component mooring line lumped mass model

The nodal forces due to added mass in the local co-ordinate were given by Eq. (2):

$$\begin{aligned} F_{A_{x_j}} &= \left(M_{A_{t_j}}\cos^2\bar{\theta}_j + M_{A_{n_j}}\sin^2\bar{\theta}_j\right)\\ &\ddot{x}_j + \left(\left(M_{A_{t_j}} - M_{A_{n_j}}\right)\sin\bar{\theta}_j\cos\bar{\theta}_j\right)\ddot{z}_j\\ F_{A_{z_j}} &= \left(\left(M_{A_{t_j}} - M_{A_{n_j}}\right)\sin\bar{\theta}_j\cos\bar{\theta}_j\right)\\ &\ddot{x}_j + \left(M_{A_{t_j}}\sin^2\bar{\theta}_j + M_{A_{n_j}}\cos^2\bar{\theta}_j\right)\ddot{z}_j \end{aligned} \quad (2)$$

Applying equilibrium conditions at node j, the external forces should balance the reactive forces as given by Eq. (3). It should be noted here that the hydrodynamic and soil reactive forces were considered as external forces and transferred to the RHS of the equilibrium equation with negative signs. This will be discussed in detail later:

$$\begin{aligned} &\left(\overline{M}_{x_j} + M_{A_{t_j}}\cos^2\bar{\theta}_j + M_{A_{n_j}}\sin^2\bar{\theta}_j\right)\\ &\ddot{x}_j + \left(\left(M_{A_{t_j}} - M_{A_{n_j}}\right)\sin\bar{\theta}_j\cos\bar{\theta}_j\right)\ddot{z}_j = F_{x_j}\\ &\left(\left(M_{A_{t_j}} - M_{A_{n_j}}\right)\sin\bar{\theta}_j\cos\bar{\theta}_j\right)\\ &\ddot{x}_j + \left(\overline{M}_{z_j} + M_{A_{t_j}}\sin^2\bar{\theta}_j + M_{A_{n_j}}\cos^2\bar{\theta}_j\right)\ddot{z}_j = F_{z_j} \end{aligned} \quad (3)$$

Letting:

$$\begin{aligned} \sigma_{1_j} &= \overline{M}_{x_j} + M_{A_{t_j}}\cos^2\bar{\theta}_j + M_{A_{n_j}}\sin^2\bar{\theta}_j\\ \sigma_{2_j} &= \left(M_{A_{t_j}} - M_{A_{n_j}}\right)\sin\bar{\theta}_j\cos\bar{\theta}_j\\ \sigma_{3_j} &= \overline{M}_{z_j} + M_{A_{t_j}}\sin^2\bar{\theta}_j + M_{A_{n_j}}\cos^2\bar{\theta}_j \end{aligned} \quad (4)$$

where,

$$\begin{aligned} M_{A_{t_j}} &= \rho\frac{\pi}{8}C_{At}\left(D^2_{j-\frac{1}{2}}L_{j-\frac{1}{2}} + D^2_{j+\frac{1}{2}}L_{j+\frac{1}{2}}\right)\\ M_{A_{n_j}} &= \rho\frac{\pi}{8}C_{An}\left(D^2_{j-\frac{1}{2}}L_{j-\frac{1}{2}} + D^2_{j+\frac{1}{2}}L_{j+\frac{1}{2}}\right)\\ M_j &= \frac{1}{2}\left(m_{j-\frac{1}{2}}L_{j-\frac{1}{2}} + m_{j+\frac{1}{2}}L_{j+\frac{1}{2}}\right)\\ M_{A_{x\,att_j}} &= C_{A_x}\rho V_{att_j}\\ M_{A_{z\,att_j}} &= C_{A_z}\rho V_{att_j} \end{aligned} \quad (5)$$

The ODEs given in Eq. (3) could be written in a simple matrix form as given by Eq. (6), which represented the GEOM of the studied MCML**:**

$$\begin{bmatrix} \sigma_{1_j} & \sigma_{2_j}\\ \sigma_{2_j} & \sigma_{3_j} \end{bmatrix}\begin{Bmatrix} \ddot{x}_j\\ \ddot{z}_j \end{Bmatrix} = \begin{Bmatrix} F_{x_j}\\ F_{z_j} \end{Bmatrix} \quad (6)$$

The external forces considered were the element tensions above and below the node, the nodal lumped submerged weight of, the weight of node attachment (if applicable), the global fluid loading due to drag force on the node adjacent elements and due to drag concentrated on node attachment. By evaluating the external force components along the global co-ordinate reference axis system, the RHS of Eq. (3) was given by Eq. (7):

$$\begin{aligned} F_{x_j} &= T_{j+\frac{1}{2}}\cos\theta_{j+\frac{1}{2}} - T_{j-\frac{1}{2}}\cos\theta_{j-\frac{1}{2}} - \bar{f}_{x_j}\\ F_{z_j} &= T_{j+\frac{1}{2}}\sin\theta_{j+\frac{1}{2}} - T_{j-\frac{1}{2}}\sin\theta_{j-\frac{1}{2}} - \bar{f}_{z_j} \end{aligned} \quad (7)$$

where,

$$\bar{f}_{x_j} = \left(f_{x_j} + f_{x_{att_j}}\right)$$

$$\bar{f}_{z_j} = \left(f_{z_j} + f_{z_{att_j}} + W_j + W_{att_j} + f_{z_{soil}} \right)$$
$$W_j = \frac{1}{2}\left(\omega_{j-\frac{1}{2}} L_{j-\frac{1}{2}} + \omega_{j+\frac{1}{2}} L_{j+\frac{1}{2}} \right) \quad (8)$$

Substituting Eq. (8) into Eq. (3) to obtain Eq. (9):

$$\begin{bmatrix} \sigma_{1_j} & \sigma_{2_j} \\ \sigma_{2_j} & \sigma_{3_j} \end{bmatrix} \begin{Bmatrix} \ddot{x}_j \\ \ddot{z}_j \end{Bmatrix} = \begin{Bmatrix} T_{j+\frac{1}{2}} \cos\theta_{j+\frac{1}{2}} - T_{j-\frac{1}{2}} \cos\theta_{j-\frac{1}{2}} - \bar{f}_{x_j} \\ T_{j+\frac{1}{2}} \sin\theta_{j+\frac{1}{2}} - T_{j-\frac{1}{2}} \sin\theta_{j-\frac{1}{2}} - \bar{f}_{z_j} \end{Bmatrix} \quad (9)$$

Fluid forces were evaluated through the application of Morison's equation to each element as though it was a smooth cylinder. This was initially calculated in a local axes' system and then the fluid loading in global co-ordinate system was evaluated through the application of the standard rotation transformation procedure. In addition to the drag on the line elements, there was also the hydro-dynamic drag on any concentrated substance attached to the mooring line such as spring buoy or clump weight. The procedure for evaluation of fluid drag forces was as follows:

- Evaluation of relative fluid/line nodal velocities in global co-ordinate system as given by Eq. (10):

$$\left.\begin{aligned} r_{x_j} &= \dot{x}_j - (u_j + c_j) \\ r_{z_j} &= \dot{z}_j - v_j \end{aligned}\right\} \quad (10)$$

The Airy's linear wave theory (Chakrabarti, 1987) was adopted for evaluation of the wave velocities as given in Eq. (16). The wave length in Eq. (11) was obtained using an iterative technique applying the dispersion relation given in Eq. (12):

$$u_j = \frac{\pi H}{T_w} \frac{\cosh\left(k_w\left(d - Z_j\right)\right)}{\sinh\left(k_w d\right)} \cos\left(k_w X_j - \omega t\right)$$
$$v_j = \frac{\pi H}{T_w} \frac{\sinh\left(k_w\left(d - Z_j\right)\right)}{\sinh\left(k_w d\right)} \sin\left(k_w X_j - \omega t\right) \quad (11)$$

$$L_w = \frac{g T_w^2}{2\pi} \tanh\left(k_w d\right) \quad (12)$$

- Transformation of the nodal relative velocities to local axes using the element orientation angle average angles as given by Eq. (13):

$$r_{t_1}{}_{j-\frac{1}{2}} = r_{x_{j-1}} \cos\theta_{j-\frac{1}{2}} + r_{z_{j-1}} \sin\theta_{j-\frac{1}{2}}$$
$$r_{t_2}{}_{j-\frac{1}{2}} = r_{x_j} \cos\theta_{j-\frac{1}{2}} + r_{z_j} \sin\theta_{j-\frac{1}{2}}$$
$$r_{n_1}{}_{j-\frac{1}{2}} = r_{z_{j-1}} \cos\theta_{j-\frac{1}{2}} - r_{x_{j-1}} \sin\theta_{j-\frac{1}{2}}$$
$$r_{n_2}{}_{j-\frac{1}{2}} = r_{z_j} \cos\theta_{j-\frac{1}{2}} - r_{x_j} \sin\theta_{j-\frac{1}{2}} \quad (13)$$

- Evaluation of the fluid reactive forces per unit length for line elements in local co-ordinates assuming that nodal orientations were equal to the adjacent element orientations as given by Eq. (14):

$$P_{t_1}{}_{j-\frac{1}{2}} = \frac{\rho}{2} C_{D_t} D_{j-\frac{1}{2}} \left| r_{t_1}{}_{j-\frac{1}{2}} \right| r_{t_1}{}_{j-\frac{1}{2}}$$
$$P_{t_2}{}_{j-\frac{1}{2}} = \frac{\rho}{2} C_{D_t} D_{j-\frac{1}{2}} \left| r_{t_2}{}_{j-\frac{1}{2}} \right| r_{t_2}{}_{j-\frac{1}{2}}$$
$$P_{n_1}{}_{j-\frac{1}{2}} = \frac{\rho}{2} C_{D_n} D_{j-\frac{1}{2}} \left| r_{n_1}{}_{j-\frac{1}{2}} \right| r_{n_1}{}_{j-\frac{1}{2}}$$
$$P_{n_2}{}_{j-\frac{1}{2}} = \frac{\rho}{2} C_{D_n} D_{j-\frac{1}{2}} \left| r_{n_2}{}_{j-\frac{1}{2}} \right| r_{n_2}{}_{j-\frac{1}{2}} \quad (14)$$

- Evaluation of member end resultant fluid forces, assuming linear force/length variation through nodes, as given by Eq. (15):

$$f_{n_1}{}_{j-\frac{1}{2}} = \frac{L_{j-\frac{1}{2}}}{6}\left(2P_{n_1}{}_{j-\frac{1}{2}} + P_{n_2}{}_{j-\frac{1}{2}} \right)$$
$$f_{n_2}{}_{j-\frac{1}{2}} = \frac{L_{j-\frac{1}{2}}}{6}\left(P_{n_1}{}_{j-\frac{1}{2}} + 2P_{n_2}{}_{j-\frac{1}{2}} \right)$$
$$f_{n_1}{}_{j+\frac{1}{2}} = \frac{L_{j+\frac{1}{2}}}{6}\left(2P_{n_1}{}_{j+\frac{1}{2}} + P_{n_2}{}_{j+\frac{1}{2}} \right)$$
$$f_{n_2}{}_{j+\frac{1}{2}} = \frac{L_{j+\frac{1}{2}}}{6}\left(P_{n_1}{}_{j+\frac{1}{2}} + 2P_{n_2}{}_{j+\frac{1}{2}} \right)$$
$$f_{t_1}{}_{j-\frac{1}{2}} = \frac{L_{j-\frac{1}{2}}}{6}\left(2P_{t_1}{}_{j-\frac{1}{2}} + P_{t_2}{}_{j-\frac{1}{2}} \right)$$
$$f_{t_2}{}_{j-\frac{1}{2}} = \frac{L_{j-\frac{1}{2}}}{6}\left(P_{t_1}{}_{j-\frac{1}{2}} + 2P_{t_2}{}_{j-\frac{1}{2}} \right)$$
$$f_{t_1}{}_{j+\frac{1}{2}} = \frac{L_{j+\frac{1}{2}}}{6}\left(2P_{t_1}{}_{j+\frac{1}{2}} + P_{t_2}{}_{j+\frac{1}{2}} \right)$$
$$f_{t_2}{}_{j+\frac{1}{2}} = \frac{L_{j+\frac{1}{2}}}{6}\left(P_{t_1}{}_{j+\frac{1}{2}} + 2P_{t_2}{}_{j+\frac{1}{2}} \right) \quad (15)$$

Evaluation of resultant nodal forces in local coordinates system as given by Eq. (16), then using the standard transformation matrix to evaluate the nodal resultant fluid forces in the global axis system and in case of available nodal attachment, the drag on attachment added to the lumped nodal drag as given by Eq. (17):

Table 1: Sea bed soils data

Designation	Type	Ø (°)	γ (kN/m^3)	C(KPa)	k_{soil} (Pa)
Soil A-1	Sand	35	18	0	4500
Soil A-2	Silty Sand	30	19	0	2600
Soil B-1	Clay	0	20	15	150

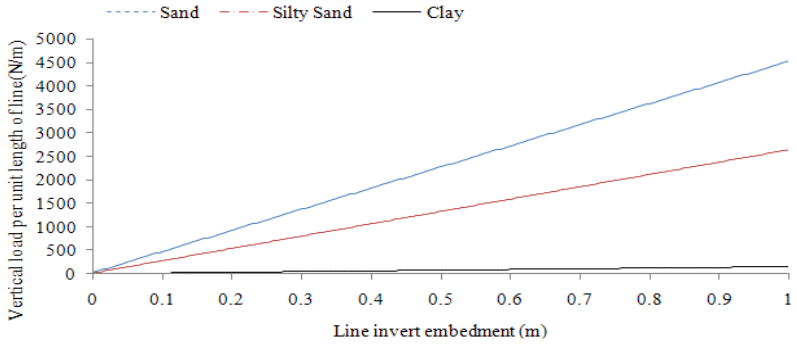

Fig. 2: Seabed soils vertical reaction per line embedment

$$F_{t_j} = f_{t_{2_{j-\frac{1}{2}}}} + f_{t_{1_{j+\frac{1}{2}}}}$$
$$F_{n_j} = f_{n_{2_{j-\frac{1}{2}}}} + f_{n_{1_{j+\frac{1}{2}}}} \quad (16)$$

$$\begin{Bmatrix} f_{x_j} \\ f_{z_j} \end{Bmatrix} = \begin{bmatrix} \cos\bar{\theta}_j & -\sin\bar{\theta}_j \\ \sin\bar{\theta}_j & \cos\bar{\theta}_j \end{bmatrix} \begin{Bmatrix} F_{t_j} \\ F_{n_j} \end{Bmatrix} + \frac{\rho}{2} \begin{Bmatrix} A_{r_x} C_{D_x} \left|r_{x_j}\right| r_{x_j} \\ A_{r_z} C_{D_z} \left|r_{z_j}\right| r_{z_j} \end{Bmatrix} \quad (17)$$

- **Seabed/ line interactions:** About 15 years ago, the US navy initiated an effort to study the static and dynamic analysis of mooring lines. Preliminary analysis results conducted by the Navy indicated that the resulting mooring line forces using some form of soil-structure interaction were less than those evaluated assuming fixed end conditions (Wung *et al*., 1994). Meanwhile, intensive work was done on seabed-risers/pipelines' interactions. Andrew (2008) extended the analysis of the pipe-laying on a rigid-plastic seabed and confirmed the field observation that large indentations occurred, particularly when the tension was low. A laboratory testing program was initiated by Clukey *et al*. (2008) to investigate potential changes in stiffness for soils in the TDP region of a steel catenary riser. Hodder and Byrne (2010) introduced a form for the nonlinear soil reaction for SCR pipe lying on a bed of sand numerically and experimentally based on an exact soil bearing capacity following Martin (2005) calculations. Hodder's soil interaction model represented a benchmark work for future studies on seabed/line interactions.

Seabed interaction was assessed as belonging to one of two scenarios: the frictional effects between the sea-bed and the mooring line and the Lifting and Grounding (L/G) interactions.

The first scenario was a physical effect usually considered in case of relatively long grounded lines (e.g., pipelines). With very little literature dealing directly with seabed friction on mooring lines such as given by Liu and Bergdashl (1997), soil friction effect was neglected in this study.

The second scenario was a modelling problem which played an important role in the mooring line dynamic response system (Gobat and Grosenbaugh, 2001). Three basic approaches were used to model this bottom interaction in numerical simulations. The first approach was to cut the mooring off at the TDP and attach an equivalent linear spring and/or dashpot, which was used in frequency domain models (Ong and Pellegrino, 2003) and in some time domain models (Teng and Wang, 1995). This approach was valid for small dynamic motions about the static TDP. The second approach was lift-off and grounding approach introduced by Nakajima *et al*. (1982) and modified by Thomas and Hearn (1994). In this method, the grounded part of the mooring line was neglected and the masses of the nodes approaching the seabed were reduced in order to avoid unrealistic impact. Mass modifiers based on parabolic mass distribution of the line were applied as multipliers of the lumped masses to the suspended first two nodes. These mass modifiers allowed the node grounding smoothly because the node reached the seafloor with having zero mass. This approach simulated a rigid bottom with no impact allowed to occur (especially for nodes attached with clump weight) and a smooth rolling and unrolling of the cable. The third approach was to model the seabed as an elastic foundation. This was used by Boom (1985), Gobat and Grosenbaugh (2001) and Inoue and Surendran (1994). Although this model had associated difficulties in determining appropriate stiffness and damping values for a given liquefied soil, it was the most convenient model for the line/seabed interaction problem.

In this study, both seabed Nakajima and elastic foundation seabed models were considered for the purpose of investigating seabed contributions to the mooring line dynamic analysis. Assuming that the mooring line rested on elastic-dissipative bed of soil, this foundation was replaced by linear spring (having zero stiffness for line invert elevations above the soil surface, allowing the line to lift from the soil without resistance) with a dashpot as shown in Fig. 1. Thus, the soil reactive forces were estimated by Eq. (18):

$$f_{z_{soil}}=\frac{k_{soil}}{2}\left(L_{j-\frac{1}{2}}+L_{j+\frac{1}{2}}\right)z_j+\varepsilon_{soil}\dot{z}_j\sqrt{2k_{soil}\bar{M}_{z_j}\left(L_{j-\frac{1}{2}}+L_{j+\frac{1}{2}}\right)}\ \text{for } z_j<0$$

$$f_{z_{soil}}=0 \text{ for } z_j\geq 0 \tag{18}$$

The stiffness k_{soil} for the line invert elevation below the sea bed was evaluated as secant stiffness to a nominal embedment from the theoretical bearing capacity curve for a strip footing in drained soil with width equal to the contact width of the soil/ mooring line (Hodder and Byrne, 2010). Soil damping ratios ε_{soil} of 0%, 3% and 5% were assumed for the purpose of investigating their contribution to the mooring line dynamics. Three soils were examined here, the cohesive-less sand, silty-sand and cohesive clay. The mechanical properties for the selected soils were obtained from Robert (2010) and the calculated soil spring stiffness is presented in Table 1. The Terzaghi's equation for the soil bearing capacity (Martin, 2005) given in Eq. (19) was used to evaluate the soil stiffness. The bearing capacity factors N_q, N_c, and N_γ (Alexandar, 1987) are given by Eq. (20). The calculated values of vertical reaction of seabed soil per line embedment are presented in Fig. 2:

$$q_u=cN_c+qN_q+\frac{1}{2}\gamma BN_\gamma \tag{19}$$

$$N_q=e^{\pi tan\emptyset}tan^2\left(\frac{\pi}{4}+\frac{\emptyset}{4}\right)$$
$$N_c=(N_q-1)/tan\emptyset$$
$$N_\gamma=2(N_q+1)tan\emptyset \tag{20}$$

- **Solution procedure:** To facilitate the solution, the GEOM represented in Eq. (13) were rearranged into a form of functional dependencies as given by Eq. (21):

$$\begin{Bmatrix}\ddot{x}_j\\ \ddot{z}_j\end{Bmatrix}=\frac{1}{\lambda_j}\begin{bmatrix}\sigma_{3_j} & -\sigma_{2_j}\\ -\sigma_{2_j} & \sigma_{1_j}\end{bmatrix}\begin{Bmatrix}T_{j+\frac{1}{2}}\cos\theta_{j+\frac{1}{2}}-T_{j-\frac{1}{2}}\cos\theta_{j-\frac{1}{2}}-\bar{f}_{x_j}\\ T_{j+\frac{1}{2}}\sin\theta_{j+\frac{1}{2}}-T_{j-\frac{1}{2}}\sin\theta_{j-\frac{1}{2}}-\bar{f}_{z_j}\end{Bmatrix}\frac{\Delta t^2}{\Delta t^2} \tag{21}$$

where,

$$\lambda_j=\sigma_{1_j}\sigma_{3_j}-{\sigma_{2_j}}^2 \tag{22}$$

Rearranging Eq. (21) in the form given by Eq. (23~24):

$$\ddot{x}_j=\frac{\Delta t^2}{\lambda_j}\begin{bmatrix}\sigma_{3_j}\left(T_{j+\frac{1}{2}}\cos\theta_{j+\frac{1}{2}}-T_{j-\frac{1}{2}}\cos\theta_{j-\frac{1}{2}}-\bar{f}_{x_j}\right)\\ -\sigma_{2_j}\left(T_{j+\frac{1}{2}}\sin\theta_{j+\frac{1}{2}}-T_{j-\frac{1}{2}}\sin\theta_{j-\frac{1}{2}}-\bar{f}_{z_j}\right)\end{bmatrix}/\Delta t^2$$

$$\ddot{x}_j=\begin{bmatrix}\frac{\Delta t^2}{\lambda_j}\left(\sigma_{3_j}\cos\theta_{j+\frac{1}{2}}-\sigma_{2_j}\sin\theta_{j+\frac{1}{2}}\right)\\ T_{j+\frac{1}{2}}-\frac{\Delta t^2}{\lambda_j}\left(\sigma_{3_j}\cos\theta_{j-\frac{1}{2}}-\sigma_{2_j}\sin\theta_{j-\frac{1}{2}}\right)\\ T_{j-\frac{1}{2}}+\frac{\Delta t^2}{\lambda_j}\left(\sigma_{2_j}\bar{f}_{z_j}-\sigma_{3_j}\bar{f}_{x_j}\right)\end{bmatrix}/\Delta t^2 \tag{23}$$

$$\ddot{z}_j=\frac{\Delta t^2}{\lambda_j}\begin{bmatrix}\sigma_{1_j}\left(T_{j+\frac{1}{2}}\sin\theta_{j+\frac{1}{2}}-T_{j-\frac{1}{2}}\sin\theta_{j-\frac{1}{2}}-\bar{f}_{z_j}\right)\\ -\sigma_{2_j}\left(T_{j+\frac{1}{2}}\cos\theta_{j+\frac{1}{2}}-T_{j-\frac{1}{2}}\cos\theta_{j-\frac{1}{2}}-\bar{f}_{x_j}\right)\end{bmatrix}/\Delta t^2$$

$$\ddot{z}_j=\begin{bmatrix}\frac{\Delta t^2}{\lambda_j}\left(\sigma_{1_j}\sin\theta_{j+\frac{1}{2}}-\sigma_{2_j}\cos\theta_{j+\frac{1}{2}}\right)\\ T_{j+\frac{1}{2}}-\frac{\Delta t^2}{\lambda_j}\left(\sigma_{1_j}\sin\theta_{j-\frac{1}{2}}-\sigma_{2_j}\cos\theta_{j-\frac{1}{2}}\right)\\ T_{j-\frac{1}{2}}+\frac{\Delta t^2}{\lambda_j}\left(\sigma_{2_j}\bar{f}_{x_j}-\sigma_{1_j}\bar{f}_{z_j}\right)\end{bmatrix}/\Delta t^2 \tag{24}$$

Letting:

$$\alpha_j=\frac{\Delta t^2}{\lambda_j}\left(\sigma_{3_j}\cos\theta_{j+\frac{1}{2}}-\sigma_{2_j}\sin\theta_{j+\frac{1}{2}}\right)$$
$$\beta_j=\frac{\Delta t^2}{\lambda_j}\left(\sigma_{3_j}\cos\theta_{j-\frac{1}{2}}-\sigma_{2_j}\sin\theta_{j-\frac{1}{2}}\right)$$
$$\gamma_j=\frac{\Delta t^2}{\lambda_j}\left(\sigma_{1_j}\sin\theta_{j+\frac{1}{2}}-\sigma_{2_j}\cos\theta_{j+\frac{1}{2}}\right)$$
$$\kappa_j=\frac{\Delta t^2}{\lambda_j}\left(\sigma_{1_j}\sin\theta_{j-\frac{1}{2}}-\sigma_{2_j}\cos\theta_{j-\frac{1}{2}}\right)$$
$$\mu_j=\frac{\Delta t^2}{\lambda_j}\left(\sigma_{2_j}\bar{f}_{z_j}-\sigma_{3_j}\bar{f}_{x_j}\right)$$
$$\psi_j=\frac{\Delta t^2}{\lambda_j}\left(\sigma_{2_j}\bar{f}_{x_j}-\sigma_{1_j}\bar{f}_{z_j}\right) \tag{25}$$

The GEOM were solved as shown by Eq. (26):

$$\ddot{x}_j=\left[\alpha_jT_{j+\frac{1}{2}}-\beta_jT_{j-\frac{1}{2}}+\mu_j\right]/\Delta t^2$$
$$\ddot{z}_j=\left[\gamma_jT_{j+\frac{1}{2}}-\kappa_jT_{j-\frac{1}{2}}+\psi_j\right]/\Delta t^2 \tag{26}$$

The GEOM time domain solution given by Eq. (26) needed an appropriate numerical time integration scheme. Generally, two numerical integration schemes are available for the problem solution, explicit and

implicit schemes. The general forms of the explicit/implicit schemes are given by Eq. (27~28), respectively:

$$\ddot{x}_j^{n+1} = f\left(x_j^{n+1}, x_j^n, x_j^{n-1}, ..., x_j^1\right) \quad (27)$$

$$\ddot{x}_j^{n+1} = f\left(x_j^{n+2}, x_j^{n+1}, x_j^n, ..., x_j^1\right) \quad (28)$$

The influence of different time integration implicit and explicit schemes used to solve the GEOM applicable to the mooring line was studied systematically by Hearn and Thomas (1991). The time integration schemes investigated were the Central Difference explicit scheme (CD) and three implicit schemes namely Houbolt, Wilson-θ and Newmark-β. An assessment of the stability, accuracy and the influence of time step size for each scheme were discussed. This study concluded that the CD scheme may be ruled out because it was limited to smaller time step than required for the implicit schemes. The Newmark-β scheme was not recommended by the authors for the cited problem because it produced an extremely inaccurate and irregular solution in case of lifting cable and sub-sea attachments. Also it took roughly twice computation time of other implicit schemes considered. Of the two remaining time schemes, it was found that there was a little difference in using either scheme but the Houbolt scheme needed a special starting procedure and thus it was not recommended by the authors. Of the three implicit methods, it was proven that Wilson-θ presented the smoothest solution and it was strongly recommended for the general solution of the cable dynamic problem. Depending upon previous recommendations, the Wilson-θ numerical integration scheme was adopted in this study for the solution of the GEOM of the MCMLs.

In the Wilson-θ scheme, a linear variation of acceleration was assumed over the time interval. If the time increased from t to t + τ, where ($0 \leq \tau \leq n + \theta\Delta t$) $\theta \geq 1.0$ in this study θwas taken as 1.4. It was assumed that acceleration at time t + τ was given by Eq. (29).

$$\ddot{x}_j^{n+\tau} = \ddot{x}_j^n + \frac{\tau}{\theta\Delta t}\left(\ddot{x}_j^{n+\theta\Delta t} - \ddot{x}_j^n\right) \quad (29)$$

By integration, the nodal velocities and displacements at time t + τ were given by Eq. (30-31).

$$\dot{x}_j^{n+\tau} = \dot{x}_j^n + \ddot{x}_j^n\tau + \frac{\tau^2}{2\theta\Delta t}\left(\ddot{x}_j^{n+\theta\Delta t} - \ddot{x}_j^n\right) \quad (30)$$

$$x_j^{n+\tau} = x_j^n + \dot{x}_j^n\tau + \ddot{x}_j^n\frac{\tau^2}{2} + \frac{\tau 3}{6\theta\Delta t}\left(\ddot{x}_j^{n+\theta\Delta t} - \ddot{x}_j^n\right) \quad (31)$$

Applying Eq. (30-31) at time n+ θΔt , nodal velocities and displacements were obtained as in Eq. (32~35):

$$\dot{x}_j^{n+\theta\Delta t} = \dot{x}_j^n + \frac{\theta\Delta t}{2}\left(\ddot{x}_j^{n+\theta\Delta t} + \ddot{x}_j^n\right) \quad (32)$$

$$x_j^{n+\theta\Delta t} = x_j^n + \dot{x}_j^n\theta\Delta t + \frac{(\theta\Delta t)^2}{6}\left(\ddot{x}_j^{n+\theta\Delta t} + \ddot{x}_j^n\right) \quad (33)$$

$$\dot{z}_j^{n+\theta\Delta t} = \dot{z}_j^n + \frac{\theta\Delta t}{2}\left(\ddot{z}_j^{n+\theta\Delta t} + \ddot{z}_j^n\right) \quad (34)$$

$$z_j^{n+\theta\Delta t} = z_j^n + \dot{z}_j^n\theta\Delta t + \frac{(\theta\Delta t)^2}{6}\left(\ddot{z}_j^{n+\theta\Delta t} + \ddot{z}_j^n\right) \quad (35)$$

The nonlinearities present in the GEOM solution Eq. (26) made the closed form solution impossible. Thus iterative procedure to achieve results of prescribed accuracy was adopted. The solution procedure could be broken down into the following steps:

- A state of equilibrium of the line was chosen based on initial upper end restoring forces. This could be the quasi-static condition of the mooring line found from catenary equations or numerical integration methods and must represent a consistent solution to a void instability of the solution, from which it was possible to extrapolate forward in time
- A set of tentative values for the displacements were determined for the next time step by applying Eq. (26, 33 and 35) using tentative estimate for the tensions at the next time step. For a first estimate, these were considered to be the tensions at the previous time step.
- In general, the tentative displacements obtained at time n + θΔt did not satisfy the condition that element length evaluated from the updated nodal co-ordinates should be equal to the distance calculated from the material constitutive relation (Hook's law in this case). The latter requirement formed the constraints equation for the iterative procedure. From this, a set the tension corrections could be derived and applied to the original tension estimates to obtain a second set of better tension estimates. Letting k indicate the tension related iteration index, the new tension estimate was given by Eq. (36):

$$^{k+1}T_{j-\frac{1}{2}}^{n+\theta\Delta t} = {}^{k+1}\tilde{T}_{j-\frac{1}{2}}^{n+\theta\Delta t} + \delta T_{j-\frac{1}{2}}^{n+\theta\Delta t} \quad (36)$$

Equation (36) was subjected to the iteration starting condition $^1T_{j-\frac{1}{2}}^{n+\theta\Delta t} = T_{j-\frac{1}{2}}^n$ for k = 0. The constraint equation or segment error function was formulated as given in Eq. (37):

$$
\begin{aligned}
{}^{k+1}\varepsilon_{j-\frac{1}{2}}^{n+\theta\Delta t} &= \left({}^{k+1}X_{j}^{n+\theta\Delta t} - {}^{k+1}X_{j-1}^{n+\theta\Delta t}\right)^2 \\
&+ \left({}^{k+1}Z_{j}^{n+\theta\Delta t} - {}^{k+1}Z_{j-1}^{n+\theta\Delta t}\right)^2 - \left[L_{j-\frac{1}{2}}\left(1+\frac{{}^{k+1}T_{j-\frac{1}{2}}^{n+\theta\Delta t}}{(EA)_{j-\frac{1}{2}}}\right)\right]^2
\end{aligned} \tag{37}
$$

Expanding the segment error function ${}^{k+1}\varepsilon_{j-\frac{1}{2}}^{n+\theta\Delta t}$ as a truncated first order Taylor series about: $\left({}^{k+1}T_{j-\frac{3}{2}}^{n+\theta\Delta t}, {}^{k+1}T_{j-\frac{1}{2}}^{n+\theta\Delta t}, {}^{k+1}T_{j+\frac{1}{2}}^{n+\theta\Delta t}\right)$ Eq. (38) was obtained:

$$
\begin{aligned}
{}^{k+1}\varepsilon_{j-\frac{1}{2}}^{n+\theta\Delta t} &= {}^{k+1}\tilde{\varepsilon}_{j-\frac{1}{2}}^{n+\theta\Delta t} + \frac{\delta^{k+1}\varepsilon_{j-\frac{1}{2}}^{n+\theta\Delta t}}{\delta^{k+1}T_{j-\frac{3}{2}}^{n+\theta\Delta t}}\delta^{k+1}T_{j-\frac{3}{2}}^{n+\theta\Delta t} \\
&+ \frac{\delta^{k+1}\varepsilon_{j-\frac{1}{2}}^{n+\theta\Delta t}}{\delta^{k+1}T_{j-\frac{1}{2}}^{n+\theta\Delta t}}\delta^{k+1}T_{j-\frac{1}{2}}^{n+\theta\Delta t} + \frac{\delta^{k+1}\varepsilon_{j-\frac{1}{2}}^{n+\theta\Delta t}}{\delta^{k+1}T_{j+\frac{1}{2}}^{n+\theta\Delta t}}\delta^{k+1}T_{j+\frac{1}{2}}^{n+\theta\Delta t} + \ldots = 0
\end{aligned} \tag{38}
$$

If the tension tentative values ${}^{k+1}\tilde{T}_{j-\frac{1}{2}}^{n+\theta\Delta t}$ were sufficiently close to the correct values, ${}^{k+1}T_{j-\frac{1}{2}}^{n+\theta\Delta t}$ it was possible to neglect the higher terms in Eq. (38) without a significant error.

- Updating nodal coordinates at time n+ θΔt by adding the nodal displacements Eq. (33 and 35) to the original nodal coordinates, Eq. (39) was obtained:

$$
\begin{aligned}
f_1\left(T_{j+\frac{1}{2}}, T_{j-\frac{1}{2}}\right) &= {}^{k+1}X_{j}^{n+\theta\Delta t} = X_{j}^{n} + \dot{x}_{j}^{n}\theta\Delta t \\
&+ \frac{(\theta\Delta t)^2}{3}\ddot{x}_{j}^{n} + \frac{\theta^2}{6}\left(\alpha_j T_{j+\frac{1}{2}} - \beta_j T_{j-\frac{1}{2}} + \mu_j\right)
\end{aligned}
$$

$$
\begin{aligned}
f_2\left(T_{j-\frac{1}{2}}, T_{j-\frac{3}{2}}\right) &= {}^{k+1}X_{j-1}^{n+\theta\Delta t} = X_{j-1}^{n} + \dot{x}_{j-1}^{n}\theta\Delta t \\
&+ \frac{(\theta\Delta t)^2}{3}\ddot{x}_{j-1}^{n} + \frac{\theta^2}{6}\left(\alpha_{j-1} T_{j-\frac{1}{2}} - \beta_{j-1} T_{j-\frac{3}{2}} + \mu_{j-1}\right)
\end{aligned}
$$

$$
\begin{aligned}
f_3\left(T_{j+\frac{1}{2}}, T_{j-\frac{1}{2}}\right) &= {}^{k+1}Z_{j}^{n+\theta\Delta t} = Z_{j}^{n} + \dot{z}_{j}^{n}\theta\Delta t \\
&+ \frac{(\theta\Delta t)^2}{3}\ddot{z}_{j}^{n} + \frac{\theta^2}{6}\left(\gamma_j T_{j+\frac{1}{2}} - \kappa_j T_{j-\frac{1}{2}} + \psi_j\right)
\end{aligned}
$$

$$
\begin{aligned}
f_4\left(T_{j-\frac{1}{2}}, T_{j-\frac{3}{2}}\right) &= {}^{k+1}Z_{j-1}^{n+\theta\Delta t} = Z_{j-1}^{n} + \dot{z}_{j-1}^{n}\theta\Delta t \\
&+ \frac{(\theta\Delta t)^2}{3}\ddot{z}_{j-1}^{n} + \frac{\theta^2}{6}\left(\gamma_{j-1} T_{j-\frac{1}{2}} - \kappa_{j-1} T_{j-\frac{3}{2}} + \psi_{j-1}\right)
\end{aligned} \tag{39}
$$

- The partial derivatives were evaluated Eq. (41~43) and substituted in segment error function Eq. (37), by expressing the segment error function in-terms of functions $f_1 \sim f_4$ given by Eq. (40):

$$
\begin{aligned}
{}^{k+1}\varepsilon_{j-\frac{1}{2}}^{n+\theta\Delta t} &= \left[f_1\left(T_{j+\frac{1}{2}}, T_{j-\frac{1}{2}}\right) - f_2\left(T_{j-\frac{1}{2}}, T_{j-\frac{3}{2}}\right)\right]^2 \\
&+ \left[f_3\left(T_{j+\frac{1}{2}}, T_{j-\frac{1}{2}}\right) - f_4\left(T_{j-\frac{1}{2}}, T_{j-\frac{3}{2}}\right)\right]^2 - \left[L_{j-\frac{1}{2}}\left(1+\frac{{}^{k+1}T_{j-\frac{1}{2}}^{n+\theta\Delta t}}{(EA)_{j-\frac{1}{2}}}\right)\right]^2
\end{aligned} \tag{40}
$$

$$
\frac{\delta^{k+1}\varepsilon_{j-\frac{1}{2}}^{n+\theta\Delta t}}{\delta^{k+1}T_{j-\frac{3}{2}}^{n+\theta\Delta t}} = \frac{\theta^2}{3}\left[\begin{aligned}&\left({}^{k+1}X_{j}^{n+\theta\Delta t} - {}^{k+1}X_{j-1}^{n+\theta\Delta t}\right) \\ &\beta_{j-1} + \left({}^{k+1}Z_{j}^{n+\theta\Delta t} - {}^{k+1}Z_{j-1}^{n+\theta\Delta t}\right)\kappa_{j-1}\end{aligned}\right] \tag{41}
$$

$$
\frac{\delta^{k+1}\varepsilon_{j-\frac{1}{2}}^{n+\theta\Delta t}}{\delta^{k+1}T_{j-\frac{1}{2}}^{n+\theta\Delta t}} = \left\{\begin{aligned}&\frac{\theta^2}{3}\left[\begin{aligned}&\left({}^{k+1}X_{j}^{n+\theta\Delta t} - {}^{k+1}X_{j-1}^{n+\theta\Delta t}\right)\left(\beta_j + \alpha_{j-1}\right) \\ &+\left({}^{k+1}Z_{j}^{n+\theta\Delta t} - {}^{k+1}Z_{j-1}^{n+\theta\Delta t}\right)\left(\kappa_j + \gamma_{j-1}\right)\end{aligned}\right] \\ &+\left[\frac{2L_{j-\frac{1}{2}}^2}{(EA)_{j-\frac{1}{2}}}\left(1+\frac{{}^{k+1}T_{j-\frac{1}{2}}^{n+\theta\Delta t}}{(EA)_{j-\frac{1}{2}}}\right)\right]\end{aligned}\right\} \tag{42}
$$

$$
\frac{\delta^{k+1}\varepsilon_{j-\frac{1}{2}}^{n+\theta\Delta t}}{\delta^{k+1}T_{j+\frac{1}{2}}^{n+\theta\Delta t}} = \frac{\theta^2}{3}\left[\begin{aligned}&\left({}^{k+1}X_{j}^{n+\theta\Delta t} - {}^{k+1}X_{j-1}^{n+\theta\Delta t}\right)\alpha_{j-1} \\ &+\left({}^{k+1}Z_{j}^{n+\theta\Delta t} - {}^{k+1}Z_{j-1}^{n+\theta\Delta t}\right)\gamma_{j-1}\end{aligned}\right] \tag{43}
$$

Letting:

$$
\begin{aligned}
\tilde{E}_{j}^{n+\theta\Delta t} &= \frac{\theta^2}{3}\left[\begin{aligned}&\left({}^{k+1}X_{j}^{n+\theta\Delta t} - {}^{k+1}X_{j-1}^{n+\theta\Delta t}\right) \\ &\beta_{j-1} + \left({}^{k+1}Z_{j}^{n+\theta\Delta t} - {}^{k+1}Z_{j-1}^{n+\theta\Delta t}\right)\kappa_{j-1}\end{aligned}\right] \\
\tilde{F}_{j}^{n+\theta\Delta t} &= \left\{\begin{aligned}&\frac{\theta^2}{3}\left[\begin{aligned}&\left({}^{k+1}X_{j}^{n+\theta\Delta t} - {}^{k+1}X_{j-1}^{n+\theta\Delta t}\right)\left(\beta_j + \alpha_{j-1}\right) \\ &+\left({}^{k+1}Z_{j}^{n+\theta\Delta t} - {}^{k+1}Z_{j-1}^{n+\theta\Delta t}\right)\left(\kappa_j + \gamma_{j-1}\right)\end{aligned}\right] \\ &+\left[\frac{2L_{j-\frac{1}{2}}^2}{(EA)_{j-\frac{1}{2}}}\left(1+\frac{{}^{k+1}T_{j-\frac{1}{2}}^{n+\theta\Delta t}}{(EA)_{j-\frac{1}{2}}}\right)\right]\end{aligned}\right\} \\
\tilde{G}_{j}^{n+\theta\Delta t} &= \frac{\theta^2}{3}\left[\begin{aligned}&\left({}^{k+1}X_{j}^{n+\theta\Delta t} - {}^{k+1}X_{j-1}^{n+\theta\Delta t}\right) \\ &\alpha_{j-1} + \left({}^{k+1}Z_{j}^{n+\theta\Delta t} - {}^{k+1}Z_{j-1}^{n+\theta\Delta t}\right)\gamma_{j-1}\end{aligned}\right]
\end{aligned} \tag{44}
$$

Equation (38) was written in the form of Eq. (45):

$$
\begin{aligned}
&\tilde{E}_{j}^{n+\theta\Delta t}\delta T_{j-\frac{3}{2}}^{n+\theta\Delta t} - \tilde{F}_{j}^{n+\theta\Delta t}\delta^{k+1}T_{j-\frac{1}{2}}^{n+\theta\Delta t} \\
&+ \tilde{G}_{j}^{n+\theta\Delta t}\delta^{k+1}T_{j+\frac{1}{2}}^{n+\theta\Delta t} = -{}^{k+1}\tilde{\varepsilon}_{j-\frac{1}{2}}^{n+\theta\Delta t}
\end{aligned} \tag{45}
$$

- A linear system of simultaneous equations was derived in Eq. (45), to solve for the tension corrections $\delta^{k+1}T_{j-\frac{1}{2}}^{n+\theta\Delta t}$. The solution of Eq. (45) was made by Gauss's elimination with backward or forward substitution algorithm but

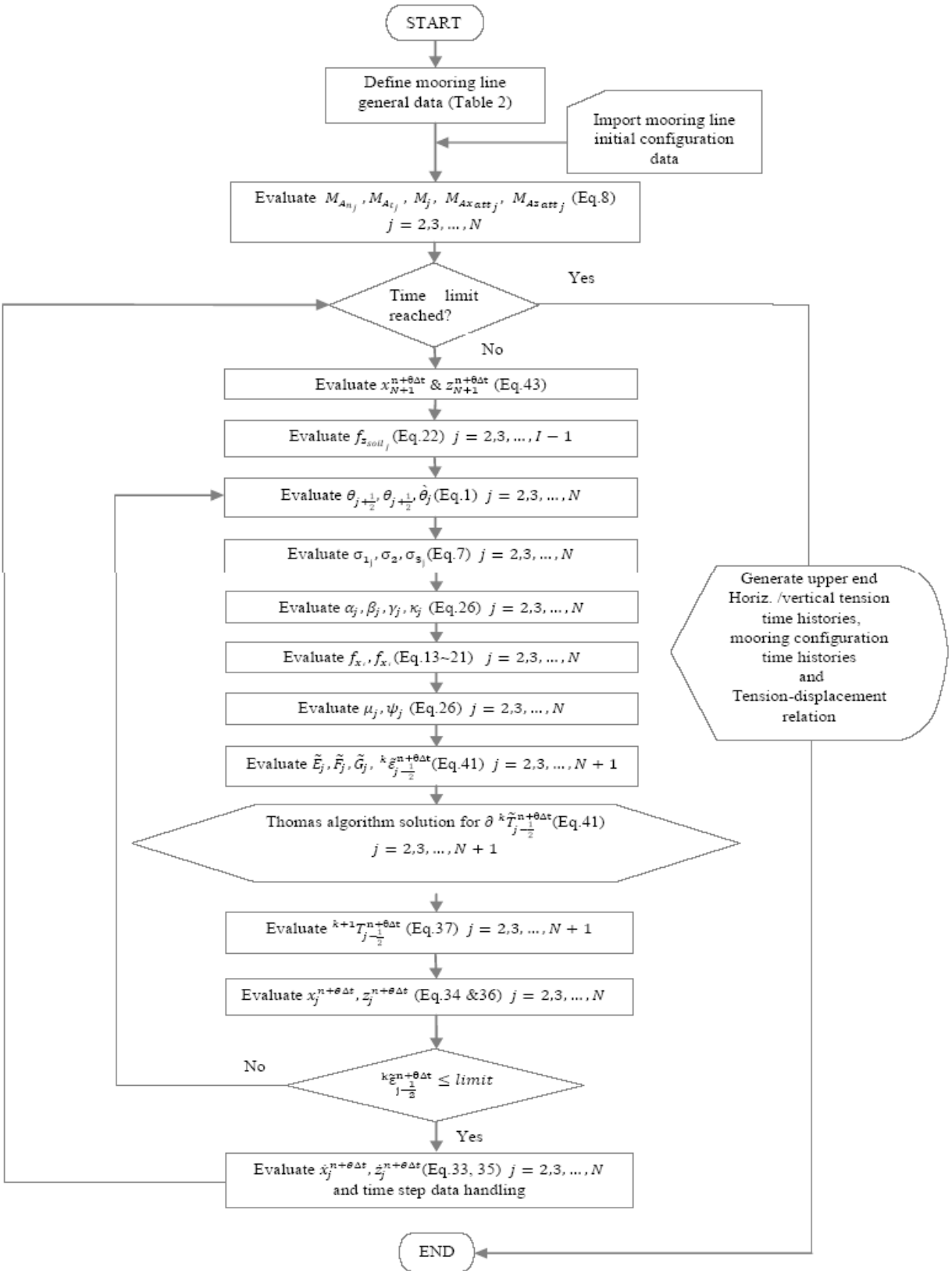

Fig. 3: Mooring line dynamic analysis flow chart

being a tri-diagonal system, it was recommended by Boom (1985) to use Thomas algorithm for efficient computations. Substituting the tension corrections in Eq. (36), better estimates of ${}^{k+1}T^{n+\theta\Delta t}$

$_{j-½}$ were obtained and used with Eq. (26, 33 and 35) to gain an improved estimate of the nodal displacement vectors $x_j^{n+\theta\Delta t}$ and $z^{n+\theta\Delta t}{}_j$. These were used to update the nodal co-ordinates and the element error functions. This procedure was continued until the latter functions achieved the desired accuracy. In this study, the accepted error in the element length was ± 1 mm:

$$\begin{bmatrix} -\tilde{F}_2^{n+\theta\Delta t} & \tilde{G}_2^{n+\theta\Delta t} & & & & & & \\ \tilde{E}_3^{n+\theta\Delta t} & -\tilde{F}_3^{n+\theta\Delta t} & \tilde{G}_3^{n+\theta\Delta t} & & & & & \\ & \tilde{E}_4^{n+\theta\Delta t} & -\tilde{F}_4^{n+\theta\Delta t} & \tilde{G}_4^{n+\theta\Delta t} & & zeros & & \\ & & .. & .. & ... & & & \\ & & & .. & ... & ... & & \\ & & & & .. & ... & ... & \\ & zeros & & & \tilde{E}_{N-1}^{n+\theta\Delta t} & -\tilde{F}_{N-1}^{n+\theta\Delta t} & \tilde{G}_{N-1}^{n+\theta\Delta t} & \\ & & & & & \tilde{E}_N^{n+\theta\Delta t} & -\tilde{F}_N^{n+\theta\Delta t} & \tilde{G}_N^{n+\theta\Delta t} \\ & & & & & & \tilde{E}_{N+1}^{n+\theta\Delta t} & -\tilde{F}_{N+1}^{n+\theta\Delta t} \end{bmatrix} \begin{Bmatrix} \delta T_1^{n+\theta\Delta t} \\ \delta T_2^{n+\theta\Delta t} \\ \delta T_3^{n+\theta\Delta t} \\ \dots \\ \dots \\ \dots \\ \delta T_{N-2}^{n+\theta\Delta t} \\ \delta T_{N-1}^{n+\theta\Delta t} \\ \delta T_N^{n+\theta\Delta t} \end{Bmatrix} = \begin{Bmatrix} -{}^{k+1}\tilde{\varepsilon}_1^{n+\theta\Delta t} \\ -{}^{k+1}\tilde{\varepsilon}_2^{n+\theta\Delta t} \\ -{}^{k+1}\tilde{\varepsilon}_3^{n+\theta\Delta t} \\ \dots \\ \dots \\ \dots \\ {}^{k+1}\tilde{\varepsilon}_{N-2}^{n+\theta\Delta t} \\ {}^{k+1}\tilde{\varepsilon}_{N-1}^{n+\theta\Delta t} \\ {}^{k+1}\tilde{\varepsilon}_N^{n+\theta\Delta t} \end{Bmatrix} \quad (46)$$

So far, only the acceleration from the Wilson-θ scheme was used. Implicit in the coefficients of Eq. (22) were the fluid-drag/soil-impact terms in-terms of the nodal velocities. Thus the nodal velocities were evaluated one step behind the current solution time step because it was not possible to evaluate the nodal velocities at the same time as trying to evaluate nodal displacements.

For this reason the time step was small enough for better estimation of the drag force at the current time step.

- **Upper-end Boundary Condition (UBC):** Simulations started by applying a starting function to the UBC. For the mathematical model adopted for the UBC in this study, the formulae for UBC were given by Eq. (47):

$$\begin{aligned} x_{N+1}^{n+\theta\Delta t} &= \left(1-e^{-\varepsilon(n+\theta\Delta t)}\right)A_x \sin\left(w_f\left(n+\theta\Delta t\right)+\varphi_x\right) \\ z_{N+1}^{n+\theta\Delta t} &= \left(1-e^{-\varepsilon(n+\theta\Delta t)}\right)A_z \sin\left(w_f\left(n+\theta\Delta t\right)+\varphi_z\right) \end{aligned} \quad (47)$$

Programming aspects: Based on the previous mentioned mathematical formulation, a computer code was developed. The flow chart is presented in Fig. 3.

RESULTS AND DISCUSSION

Based on the mathematical formulation and the flow chart shown in Fig. 3, a numerical code named

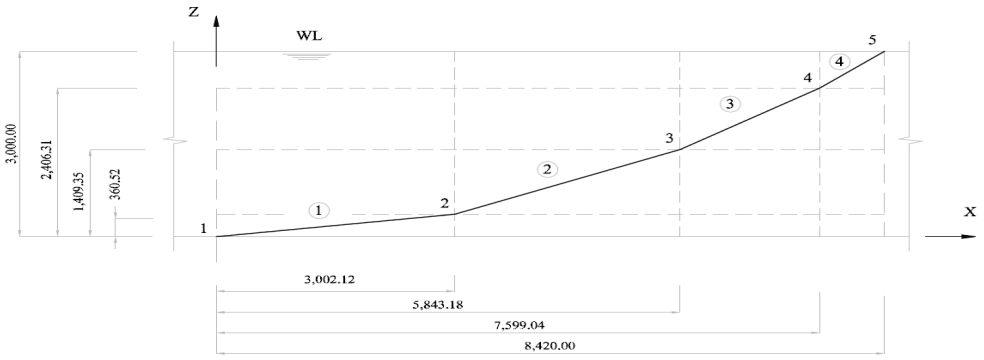

Fig. 4: Mooring No 1 initial configuration

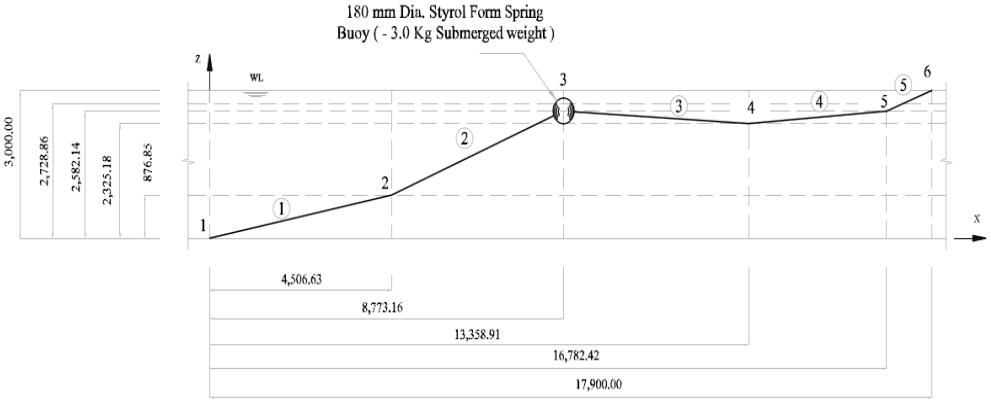

Fig. 5: Mooring No 2 initial configuration

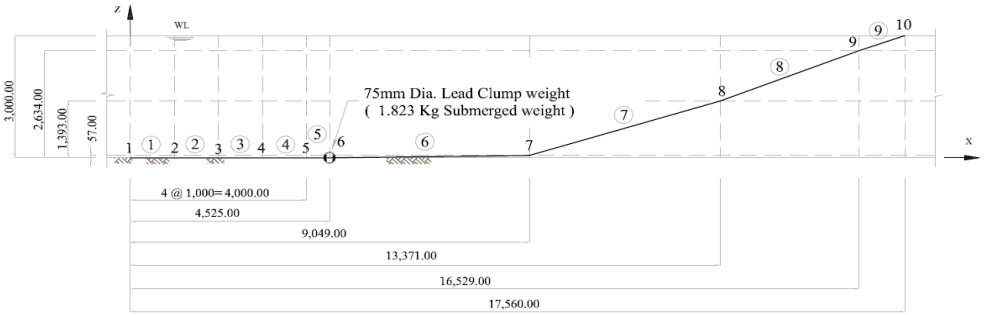

Fig. 6: Mooring No 3 initial configuration

Table 2: General data used to analyze Mooring lines No. 1-3

C_{Dn}	C_{Dt}	C_{An}	C_{At}	C_{Dx}	C_{Dz}	C_{Ax}	C_{Dz}	Δt(s)	ρ (Kg/m3)
2.18	0.17	1.98	0.20	1.00	1.00	0.50	0.50	0.02	1025

Table 3: Particulars of chain used in Mooring No. 1, 2 and 3

Submerged unit mass (Kg/m)	0.19380
Diameter (mm)	5.9900
Modulus of elasticity (Pa)	0.21085

Table 4: Mooring lines tensions

Mooring No.	Element ID	Tension (Kg)
1	1	2.539
	2	2.645
	3	2.871
	4	3.136
2	1	4.596
	2	4.809
	3	4.611
	4	4.583
	5	4.705
3	1-6	9.399
	7	9.745
	8	10.019
	9	10.317

MCMLDYN was developed in the MATLAB 2009a environment, for deepwater MCMLs dynamic analysis Three case studies were conducted for the validation of the established numerical code. The dynamic behaviour of mooring line No. 1, 2 and 3 were assessed numerically using MCMLDYN code and compared to Nakajima *et al*. (1982) experimental results. The results of mooring line No.1~3 are presented in Fig. 4 to 6 respectively, in which, the global co-ordinate system, the node numbers/coordinates, element numbers (inscribed inside circles) and concentrated weights of nodal attachments (spring buoy for mooring line No.2 and clump weight for mooring line No.3) are given. The general data used for the analysis of mooring line No. 1~3 are presented in Table 2, while the basic characteristic data for the chain used in Mooring lines No.1~3 are given in Table 3. The mooring No.1~3 element tensions are given in Table 4.

Forced oscillation tests for mooring lines No. 1~3 were conducted by Nakajima *et al*. (1982) in a wave flume containing calm water. The lower ends of the mooring lines were attached rigidly to the bottom of the model basin and the upper ends were attached to a mechanical oscillator, forced to oscillate horizontally with amplitude of 50 mm. The upper end horizontal and vertical tensions were measured by a load cell located

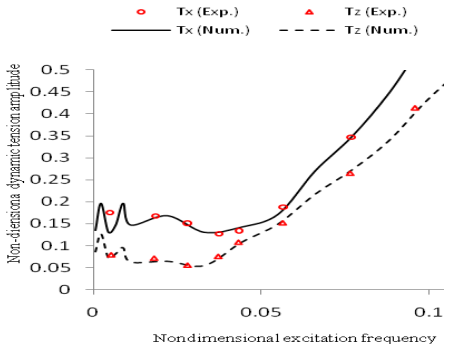

Fig. 7: Frequency response of mooring line No.1upper end dynamic tension

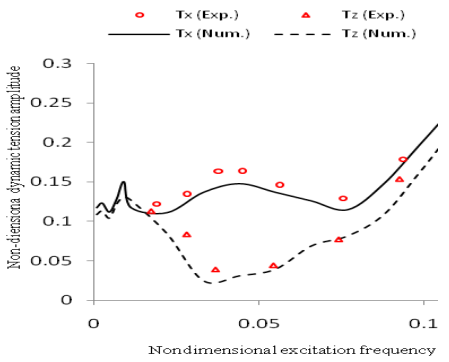

Fig. 8: Frequency response of mooring line No.2 upper end dynamic tension

at mooring line/mechanical oscillator attachment point, while the tension at the anchored point was measured by a ring gauge.

The non-dimensional tension amplitudes for the horizontal/vertical upper end dynamic tensions for mooring lines No. 1~2 Eq. (48) were plotted against the non-dimensional frequency Eq. (49) as shown in Fig. 7 and 8 respectively. It was noted that for non-dimensional frequency greater than 0.03, the dynamic tension was directly proportional to the upper end motion frequency. At the non-dimensional frequency of

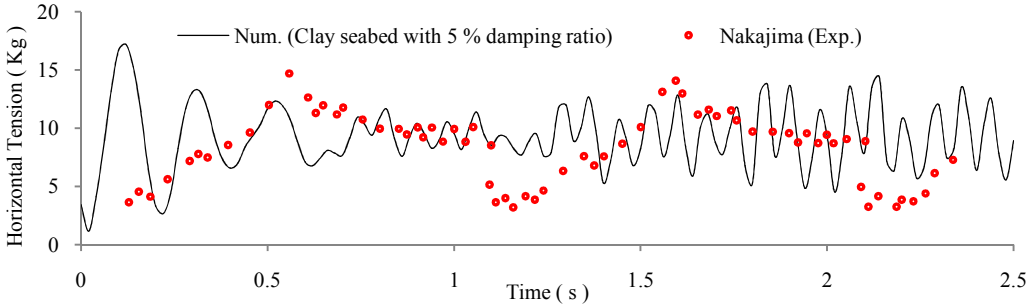

Fig. 9: Mooring line No.2 upper end horizontal dynamic tension time history

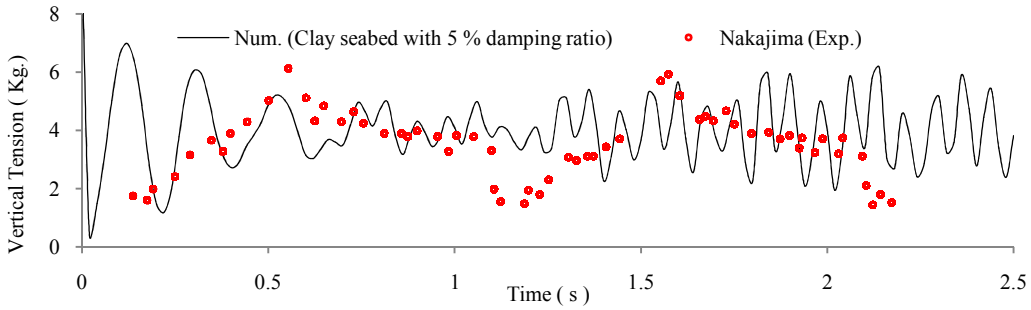

Fig. 10: Mooring line No.2 upper end vertical dynamic tension time history

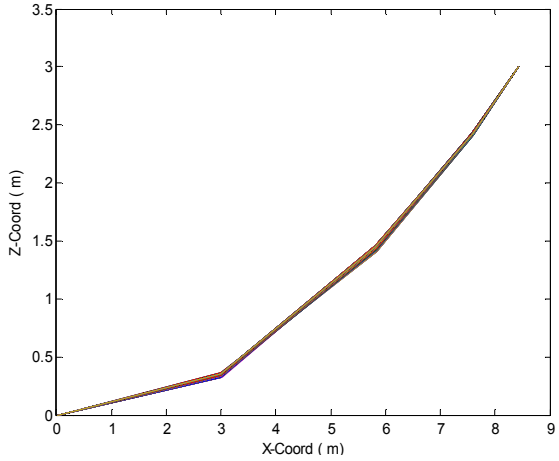

Fig. 11: Mooring line No.1 configuration time history (A_x = 50 mm, A_z =0 mm and w_f = 0.50266550 rad/sec)

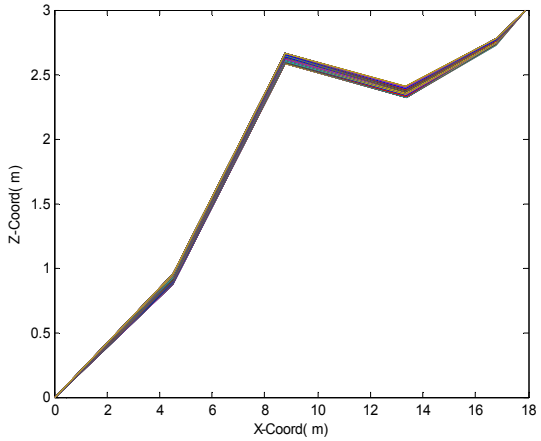

Fig. 12: Mooring line No.2 configuration time history; (A_x = 50 mm, A_z = 0 mm and w_f= 1.256637 rad/sec)

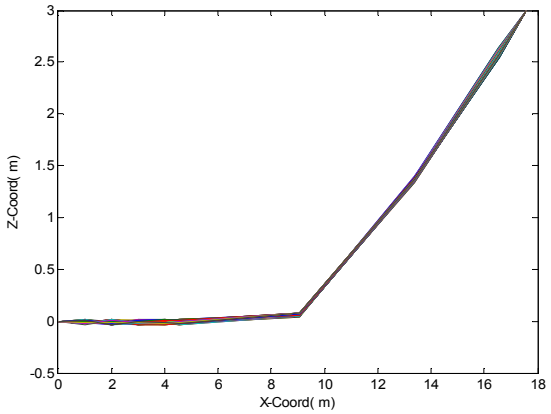

Fig. 13: Mooring line No.3 configuration time history

0.12, the dynamic tension increased about three/two times of the initial static tension for mooring lines No. 1~2 respectively. Lower increase of the dynamic tension for mooring line No.2 was due to the existence of spring buoy:

$$\overline{T}_N = \left(\frac{T_N}{2T_{o_N}} \right)$$

$$\overline{\omega}_f = \omega_f \sqrt{\frac{D_N}{2g}} \tag{48}$$

Time-domain simulations for the upper end dynamic horizontal/vertical tensions were compared to Nakajima *et al.* (1982) experimental results for upper end sinusoidal motion of 5 rad/s frequency and 50 mm amplitude with no ramp for mooring line No. 3 as shown in Fig. 9 and 10. For the numerical calculations, it was assumed that the grounded part of mooring line No. 3 rested on clay soil (Soil B.1.) having 5% damping ratio. It could be seen clearly from Fig. 12 to 15 that good agreement was achieved between the dynamic simulations of the mooring lines and Nakajima experimental results. Thus the adopted numerical model is recommended for the mooring line/seabed interactions assessment with an acceptable degree of confidence.

Fig. 11 to 13 shows the mooring line No. 1~3 configuration time history for upper end 50 mm oscillation amplitude at different frequencies in calm water. Mooring line No. 3 was assumed to be resting on clay soil (Soil B.1.), having 5% damping ratio.

To study the effect of the seabed on the line dynamics, a MCML as shown in Fig. 14 was analyzed, assuming it was lying on rigid bed (Nakajima model)

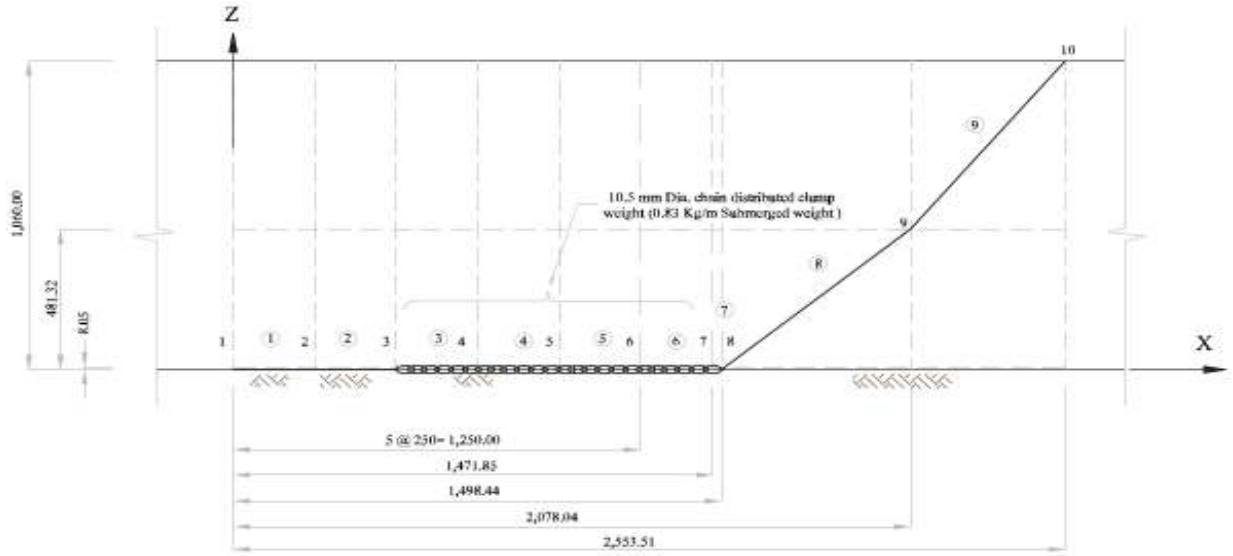

Fig. 14: A MCML with distributed clump weight

Table 5: Mooring No 4 initial configuration data

Elem, ID	D (mm)	E (GPa)	m (Kg/m)	T_o (N)	L (m)
1	1.55	3.600	0.02	0.367763	0.250000
2	1.55	3.600	0.02	0.367763	0.250000
3	10.5	3600	0.83	0.367763	0.250000
4	10.5	3600	0.83	0.367763	0.250000
5	10.5	3600	0.83	0.367763	0.250000
6	10.5	3600	0.83	0.367763	0.221850
7	10.5	3600	0.83	0.385191	0.027778
8	1.55	3.600	0.02	0.476293	0.748279
9	1.55	3.600	0.02	0.580983	0.749116

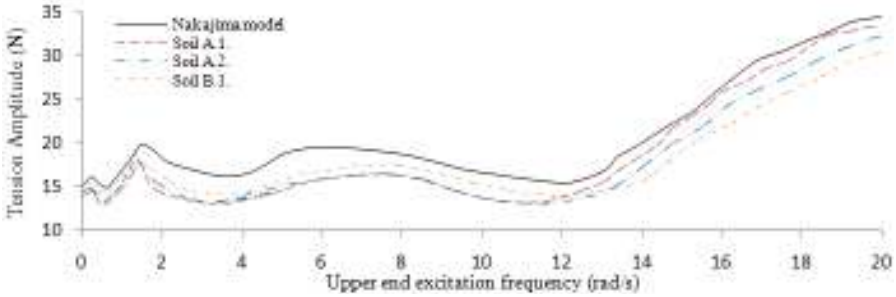

Fig. 15: Soil contribution to the horizontal dynamic restoring forces (Mooring No. 4)

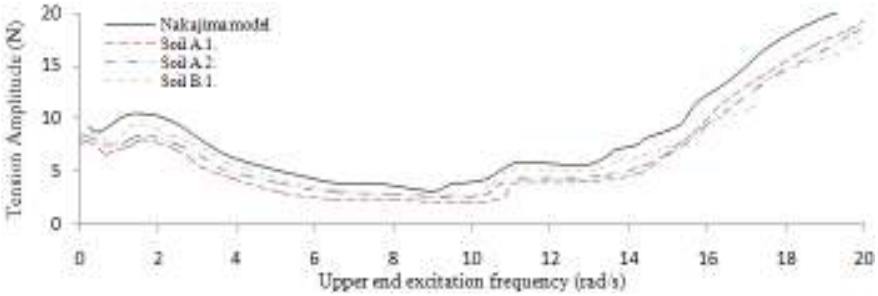

Fig. 16 Soil contribution to the vertical dynamic restoring forces (Mooring No. 4)

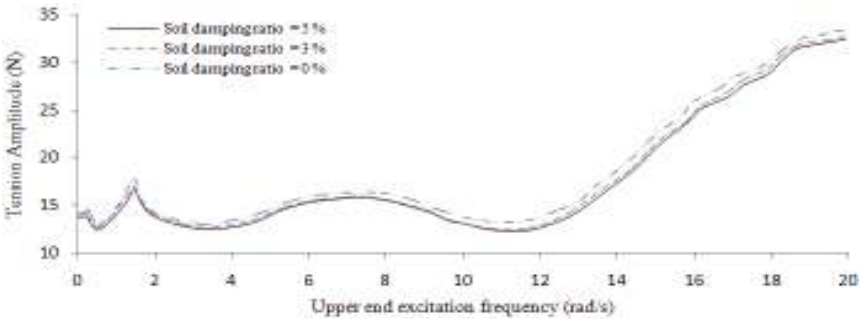

Fig. 17: Soil damping contribution to the horizontal dynamic tension (Mooring No. 4)

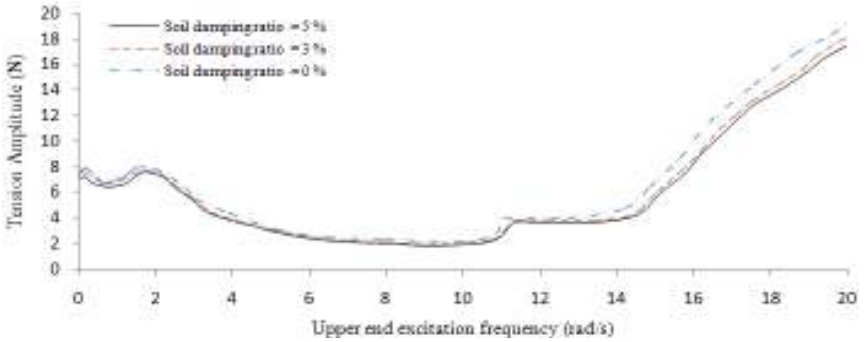

Fig. 18: Soil damping contribution to the vertical dynamic tension (Mooring No. 4)

and an elastic foundation made of clay, silty sand and sand soils with 5% damping ratio. The data for the analyzed mooring line is given in Table 5.

The horizontal and vertical tension amplitudes of the mooring line were plotted against upper end motion frequencies for a given motion amplitude of 50 mm as shown in Fig. 15 to 16. Nakajima model and elastic foundation with a dashpot were used to model the mooring line sea-bed interactions. The latter model was assumed for three different soils having the same

damping ratio of 5 %. Results showed that the elastic foundation model gave lower mooring tensions compared to Nakajima sea-bed model. It was found that for low frequencies (<12 rad/s), the second seabed model reduced the mooring tension up to 22% while for high frequencies (>12 rad/s) it reduced up to 17%. Thus elastic foundation with dashpot seabed model reduced the mooring tensions especially at low upper end motion excitation frequency.

Regarding the soil type, it was noted that for stiff soils, the mooring line tension was low at low frequencies (<12 rad/s for horizontal tension and <15 rad/sec for vertical tension), but high at high frequencies. This happened due to the high soil reactions to high frequency line dynamic actions. In other words, stiff soils provided desired effect to line dynamics (decreased tension) at low frequencies, but it had an adverse effect at high motion frequencies (increased tension).

To investigate the contribution of the soil damping to the mooring line dynamics, the mooring line No. 4 was dynamically analyzed in calm water with upper end motion having different frequencies for a given motion amplitude of 50 mm. It was assumed that the grounded part of the mooring was supported upon clay soil (Soil B.1.), which had a damping ratio of 0, 3 and 5%, respectively as shown in Fig. 17 and 18. Results indicated that the higher the soil damping, the lower the mooring tensions. Comparing un-damped soil to damped soil (5% damping ratio), a maximum of about 3% difference was obtained for horizontal tension at low frequencies (<10rad/s), while about 4% difference was obtained for horizontal tensionat high frequencies (>10 rad/s). On the other hand for the vertical tension, a maximum difference of about 7% was obtained at low frequencies (<10 rad/s) and about 9% at high frequencies (>10 rad/s) when comparing un-damped soil to damped soil (5% damping ratio). Thus the soil damping decreased vertical tensions more than horizontal tensions and decreased tensions at high frequencies more than at low frequencies.

CONCLUSION

From this study, the following conclusions were drawn:

- The developed numerical model can be used for the analysis and design of the dynamic analysis of MCMLs with an improved degree of confidence since a good agreement between numerical simulations and published experimental results was achieved.
- The mooring line dynamic tension was directly proportional to the upper end motion frequency.
- For the mooring line attached spring buoy, the rate of increase of dynamic tension with respect to frequency of mooring upper end motion was generally lower compared to that without spring buoy and was particularly lower at higher frequency of mooring upper end motion. This strengthens the well-known beneficial effect of the spring buoy.
- When soil damping and the upper end excursions were constant, the mooring line tension lowered when the soil stiffness increased.
- Compared to lifting and grounded seabed model introduced by Nakajima, elastic foundation with dashpot seabed model gave lower mooring tensions, especially at low UBC's frequency.
- For very stiff soils, the desired effect of lowering the mooring line tension was achieved at the low frequency of upper end motion, but it produced an adverse effect at the high frequency of upper end motion due to high impact.
- The soil damping dissipated the impact due to the mooring dynamic responses, which resulted in lower mooring line tensions, especially at a high frequency of the upper end motion. And due to the direction nature of the soil reactive forces, the vertical components of the mooring line tension were more affected by soil damping in comparison to the horizontal components.

ACKNOWLEDGMENT

The authors would like to gratefully acknowledge their gratitude the Universiti Teknologi PETRONAS (UTP) for the constant support and encouragement.

NOMENCLATURE

A_{r_x}, A_{r_z}	:	Projected area of the concentrated attachments in X and Z directions respectively
A_x, A_z	:	Upper end motion amplitudes in X and Z directions respectively
B	:	Foundation width
C_{A_x}, C_{A_z}	:	Added mass coefficients of the concentrated attachments in X and Z directions respectively
C_{D_n}, C_{D_t}	:	Added mass coefficients of the mooring line in normal and tangential local directions respectively
C_{D_x}, C_{D_z}	:	Fluid drag coefficients of the concentrated attachments in X and Z directions respectively
$D_{j-\frac{1}{2}}$	:	Diameter of element $j-\frac{1}{2}$
$\widetilde{E}_j$, $\widetilde{F}_j$, $\widetilde{G}_j$	:	Coefficient functions for the tension correction equations

F_{n_j}, F_{t_j} : Fluid drag force of the mooring line in normal and tangential local directions respectively lumped on node j

F_{xj}, F_{zj} : Total external force applied on node j in X and Z directions respectively

H : Propagated wave height

I : The first suspended node of the mooring line

$L_{j-\frac{1}{2}}$: Unreformed length of element $j-\frac{1}{2}$

L_w : Propagated wave length

M_j : The equivalent submerged mass of $j-\frac{1}{2}$ and $j+\frac{1}{2}$ mooring elements lumped on node j

$M_{A_{t_j}}$, $M_{A_{n_j}}$: The equivalent added mass of $j-\frac{1}{2}$ and $j+\frac{1}{2}$ mooring elements in normal and tangential local directions respectively, lumped on node j

$M_{A_{x_{att_j}}}, M_{A_{z_{att_j}}}$: Added mass of the concentrated attachments at node j in X and Zdirections respectively

M_{att_j} : Submerged mass of the concentrated attachments at node j

$\overline{M}_{x_j}$, $\overline{M}_{z_j}$: Virtual mass for node j (include the lumped submerged mass and submerged/ added mass of the concentrated attachments) in X and Z directions respectively

N_q, N_c, N_γ : Bearing capacity coefficients of the soil underlying the mooring line

$P_{n_{1_{j-\frac{1}{2}}}}, P_{t_{1_{j-\frac{1}{2}}}}$: Fluid drag force per unit length on element $j-\frac{1}{2}$ near end, in normal and tangential local directions respectively

$P_{n_{2_{j-\frac{1}{2}}}}, P_{t_{2_{j-\frac{1}{2}}}}$: Fluid drag force per unit length on element $j-\frac{1}{2}$ far end, in normal and tangential local directions respectively

T_w : Propagated wave period

$T_{j-\frac{1}{2}}$: Axial dynamic tension on element $j-\frac{1}{2}$

$\overline{T}_N$: Non-dimensional dynamic tension at the upper end of mooring line

V_{att_j} : Volume of the concentrated attachments at node j

W_j : Equivalent submerged weight of $j-\frac{1}{2}$ and $j+\frac{1}{2}$ mooring elements lumped on node j

W_{att_j} : Submerged weight of the concentrated attachments at node j

X_j, Z_j : Co-ordinates of node j in X and Z directions respectively

c_j : Current velocity at node j

c : Cohesion of the soil underlying the mooring line

d : Upper end height above sea level at the mooring initial configuration

$f_{n_{1_{j-\frac{1}{2}}}}$, $f_{t_{1_{j-\frac{1}{2}}}}$: Fluid drag force on element $j-\frac{1}{2}$ near end, in normal and tangential local directions respectively

$f_{n_{2_{j-\frac{1}{2}}}}, f_{t_{2_{j-\frac{1}{2}}}}$: Fluid drag force on element $j-\frac{1}{2}$ far end, in normal and tangential local directions respectively

f_{x_j}, f_{z_j} : Fluid drag force lumped on node j in X and Z directions respectively

$f_{x_{att_j}}$, $f_{z_{att_j}}$: Fluid drag force on attachment at node j in X and Z directions respectively

$f_{z_{soil}}$: Soil reactive force at node j in Z direction

$\bar{f}_{x_j}$, $\bar{f}_{z_j}$: Virtual external force node j (include the fluid drag force of line/attachment, weight of line attachment and soil reactive force) in X and Z directions respectively

g : Gravitational acceleration

k_w : Propagated wave number

k_{soil} : Stiffness of the soil underlying the mooring line

$m_{j-\frac{1}{2}}$: Submerged mass per unit length of element $j-\frac{1}{2}$

q : Soil overburden pressure at the mooring line level of embedment

q_u : Ultimate bearing capacity of the soil underlying the mooring line

$r_{n_{1_{j-\frac{1}{2}}}}$, $r_{t_{1_{j-\frac{1}{2}}}}$: Relative velocity on element $j-\frac{1}{2}$ near $j-\frac{1}{2}$ respectively

$r_{n_{1_{j-\frac{1}{2}}}}, r_{t_{1_{j-\frac{1}{2}}}}$: Relative velocity on element $j-\frac{1}{2}$ far end, in normal and tangential local directions respectively

r_{x_j}, r_{z_j} : Relative velocity at node j in X and Z directions respectively

t : Time

u_j, v_j : Propagated wave velocity at node j in X and Z directions respectively

x_j, z_j : Displacement of node j in X and Z directions respectively

$\dot{x}_j$, $\dot{z}_j$: Velocity of node j in X and Zdirections respectively

$\ddot{x}_j$, $\ddot{z}_j$: Acceleration of node j in X and Z directions respectively

σ_{1_j}, σ_{2_j}, σ_{3_j} : Functions used for defining the governing equation of motion

$\theta_{j-\frac{1}{2}}$: Orientation angle of element $j-\frac{1}{2}$ (Angle of element $j-\frac{1}{2}$ with the positive X-axis measured counterclockwise)

$\overline{\theta}_j$: Average angle of node j (Angle of the tangent at node j with the positive X-axis measured counterclockwise)

ρ : Fluid mass density

ω, ω_f : Frequency of the propagated wave and the upper end motion respectively

$\overline{\omega} f$: The non-dimensional frequency of the upper end motion

$\omega_{j-\frac{1}{2}}$: Submerged weight per unit length of element $j-\frac{1}{2}$

ε_{soil} : Damping ratio of the soil underlying the mooring line

γ, ϕ : Mass density and internal friction angle of the soil underlying the mooring line respectively

Δt : Time step

$\alpha_j,\beta_j,\gamma_j,\kappa_j,\mu_j,\psi_j$: Functions used to define governing equation of motion solution

θ : Constant of the adopted time integration scheme (Wilson- θ)

$\delta T^{n+\theta\Delta t}_{j-\frac{1}{2}}$: Correction of the tension at element $j-\frac{1}{2}$

$\varepsilon^{n+\theta\Delta t}_{j-\frac{1}{2}}$: Element $j-\frac{1}{2}$ error function

ε : Coefficient of the upper end motion ramp function

φ_x, φ_z : Phase angle for the upper end motion in X and Z directions respectively

REFERENCES

Alexandar, S.V., 1987. Bearing capacity of shallow foundation. Ph.D. Thesis, Civil Engineering, Duke.

Anasri, K.A., 2001. Dynamics of Offshore Vessels. School of Engineering, Washington USA.

Andrew, P., 2008. Touchdown identation of sea-bed. Appl. Ocean Res., 30: 235-238.

API, 2005. Design and Analysis of Station-keeping Systems for Floating Structures. American Petroleum Institute, Washington, D.C.

Boom, H.J., 1985. Dynamic behaviour of mooring lines. Proceeding of 4th International Conference on the Behaviour of Offshore Structures, Delft.

Chakrabarti, S.K., 1987. Hydro-dynamics of Offshore Structures. Illinois CBI Industries, Inc., Plainfield, USA.

Cho, K.N. and W.S. Yi, 2002. Developement of a dynamic analysis scheme of cable for ROV Operation. Proceedings of the 12th International Offshore and Polar Engineering Conference Kitakyushu. Japan, pp: 249-254.

Clukey, E.C., A.G. Young, G.S. Garmon and J.R. Dobias, 2008. Soil response and stiffness laboratory measurements of SCR Pipe/soil interaction. Proceeding of Offshore Technology Conference. Houston, Texas.

Gobat, J.I. and M.A. Grosenbaugh, 2001. Dynamics in the touchdown region of catenary moorings. Proceedings of the 11th International Offshore and Polar Engineering Conference. Stavanger, Norway.

Hearn, G.E. and D.O. Thomas, 1991. The influence of time integrtion schemes on dynamic mooring line analysis. Proceeding of Offshore Technology Conference. Houston, Texas.

Hodder, M.S. and B.W. Byrne, 2010. 3D experiments investigating the interaction of a model SCR with the seabed. Appl. Ocean Res., 35(2): 146-157.

Inoue, Y. and S. Surendran, 1994. Dynamics of theinteraction of mooring lines with the sea bed. Proceedings of the 4th International Offshore and Polar Engineering Conference. Osaka, Japan, pp: 317-323.

Kreuzer, E. and U. Wilke, 2003. Dynamics of mooring systems in ocean engineering. Arch. Appl. Mech., 75: 270-281.

Liu, Y. and L. Bergdashl, 1997. Influence of current and seabed friction on mooring cables: Comparison between time-domain and frequency-domain anlysis. Eng. Struct., 19: 945-953.

Martin, C.M., 2005. Exact bearing capacity calculations using the method of characteristics. Proceeding of 11th International Conference IACMAG, Turin, 4: 441-450.

Nakajima, T., 1986. Anew 3D quasi-static solution for the multi-compnent mooring systems. 5th OMAE, pp: 487-493.

Nakajima, T., S. Motora and M. Fujino, 1982. On the dynamic analysis of multi-component mooring lines. Proceeding of Offshore Technology Conference. Houston, Texas.

Ong, P.P.A. and S. Pellegrino, 2003. Modelling of seabed interaction in FD analysis mooring cables. Proceeding of ASME 2003 22nd International Conference on Offshore Mechanics and Arctic Engineering. Cancun, Mexico.

Robert, D., 2010. Foundation Engineering Handbook. McGraw Hill Professional, New York, pp: 1008, ISBN: 0071740090.

Teng, C.C. and H.T. Wang, 1995. Mooring of surface wave following buoys in shallow waters. Proceeding of 14th International Conference on Offshore Mechanics and Arctic Engng. Copenhagen, pp: 223-230.

Thomas, D.O. and G.E. Hearn, 1994. Deep water mooring line dynamics with emphasis on seabed interfenece effects. Proceeding of Offshore Technology Conference. Houston, Texas.

Walton, T.S. and M.J. Polachech, 1960. Calculation of transient motion of submerged cables. Math. Comp., 14: 27-41.

Wung, C.C., R.W. Litton, H.M. Mitwally, S. Bang and R.J. Taylor, 1994. Effect of soil on moring system dynamics. Proceeding of Offshore Technology Conference. Houston, Texas.